UNIVERSITAT POLITÈCNICA DE CATALUNYA
BARCELONATECH

MASTER THESIS

Use of electrodynamic screens for the optimization of the performance of optics and solar panels on the Moon's surface

Silvia Díaz Gilete

SUPERVISED BY

Ignasi Casanova Hormaechea

Universitat Politècnica de Catalunya
Master in Aerospace Science & Technology
March 2014

Use of electrodynamic screens for the optimization of the performance of optics and solar panels on the Moon's surface

BY

Silvia Díaz Gilete

DIPLOMA THESIS FOR DEGREE

Master in Aerospace Science and Technology

AT

Universitat Politècnica de Catalunya

SUPERVISED BY:

Ignasi Casanova

Department of Construction Engineering,
Institute of Energy Technologies and
Center for Research in Nanoengineering

ABSTRACT

The Moon is an excellent place to make astronomical observations and, furthermore, a great platform to study and gain a better understanding of our own planet and the Universe. However a thin layer of dust covers the lunar surface. It consists of electrostatically charged grains of less than 20 μm in diameter. Due to their tiny size, charge and low gravity, they remain suspended from 10 cm to high altitudes (100 km), and would eventually deposit onto solar panels and optical elements causing the degradation of their performance.

To overcome this problem, some studies have proposed the use of a quasi-transparent electromagnetic shield to facilitate the cleaning of the electrostatically charged dust from surfaces, therefore preventing its accumulation, optimizing efficiency and extending the lifetime of the instruments. These are the so-called Electrodynamic Screens (EDS) and consist of a series of parallel electrodes equally spaced and connected to an alternating current source that generates an electromagnetic wave, in movement, thus repelling the particles.

The aim of this project is to find the best configuration of the EDS (width of the electrodes, distance between them and so on) in order to achieve the maximum efficiency in removing dust. For this, the results of experiments conducted to date on the Clearing Factor (CF) or Dust Removal Efficiency (DRE) will be analyzed to determine which parameters and to what extent they affect the efficiency of dust removal in an EDS. In addition to this, the best location on the lunar surface for solar panels and telescopes according to illumination conditions and minimization of dust effects will be evaluated.

Keywords: Lunar dust mitigation, Electrodynamic screen (EDS), solar panel, optics.

Table of Contents

List of Figures

List of tables

INTRODUCTION

The Moon is an ideal place to perform astronomical observations and scientific missions allowing us to better understand the Universe and also will serve as a stepping-stone to Mars.

Nonetheless the lunar surface is covered by dust, which is a major drawback to overcome due to its abrasiveness, pervasive nature and gravitational settling on optical lens and solar cells among other instruments, degrading their performance. These dust particles are tiny (< 20 μm in diameter) and electrostatically charged, and along with the low gravity of the Moon makes the dust grains may lift up to 100 km.

For the purpose of mitigating the effects of dust and thus extending the lifetime of the instruments, it is proposed the use of Electrodynamic Screens (EDS). EDS are quasi-transparent electromagnetic shields that do not involve mechanical action or water. It consists of a series of parallel electrodes equally spaced and connected to an alternating current source that generates an electromagnetic wave, in movement, thus repelling the particles.

The goal of this project is to determine the best configuration of the EDS so as to maximize the performance of removing lunar dust. This is going to be achieved through experiments and patents conducted to date. As well, it will be assessed the best locations on the lunar surface for solar panels and telescopes according to illumination conditions and minimization of dust effects.

The main conclusions are that the AC signal that feeds the EDS and the size distribution of dust influence in the removal efficiency and in the configuration of the electrodes. Moreover, solar panels have maximum efficiency on the polar regions, while telescopes depends on their object of study. But both are better placed at 2 m, approximately, above the surface. To reach these, the paper is structured as follows:

In the first chapter, it will be explained the properties of the lunar dust and its mechanisms of transport in order to better understand how detrimental it can be for the instruments sent to the Moon, especially for solar panels and optics which provide energy to perform the mission and collect data and images for the investigation respectively.

In the second, a solution to the problem of clinging lunar dust will be proposed, consisting in the use of Electrodynamic Screens to prevent its accumulation. The state of the art of an EDS is introduced herein, its basics principles as well as how the electric field distribution, the conveyor and the electrodes are defined.

In the third chapter, all the parameters that can influence the operation of an electrodynamic screen are characterized when modeling it because they affect the removal efficiency of moon dust. These parameters serve to determine the correct and most efficient screen settings.

Finally, besides the use of electrodynamic screens, in the fourth chapter, different sites on the lunar surface are proposed to preferably place solar panels or optics, according to their purpose and to enhance their efficiency.

Chapter 1

LUNAR DUST PROBLEMATICS

1.1. What is lunar dust?

Lunar soil is the fine regolith found on the surface of the Moon and which is typically up to several meters deep. It has a broad size distribution of particles and an average grain size is of about 70 μm; over 95% is finer than 1 mm, about 50% is finer than 60 μm and 10-20% is finer than 20 μm [1].

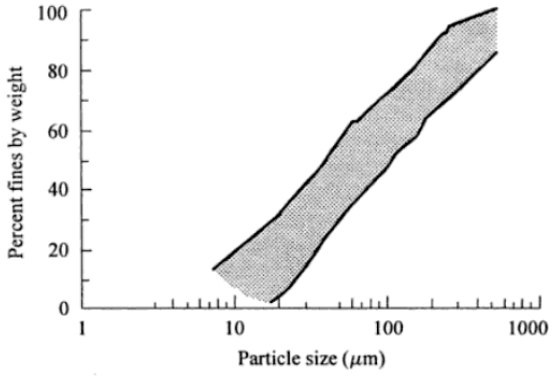

Figure 1.1 Grain size distribution from samples from Apollo 11, 12, 14 and 15 [2]

Lunar dust is defined as the fine portion of the lunar soil with a particle diameter usually less than 20 μm [3], but there is no official definition of its size, so in some places the cutoff is at less than 50 μm [1] or 100 μm [4].

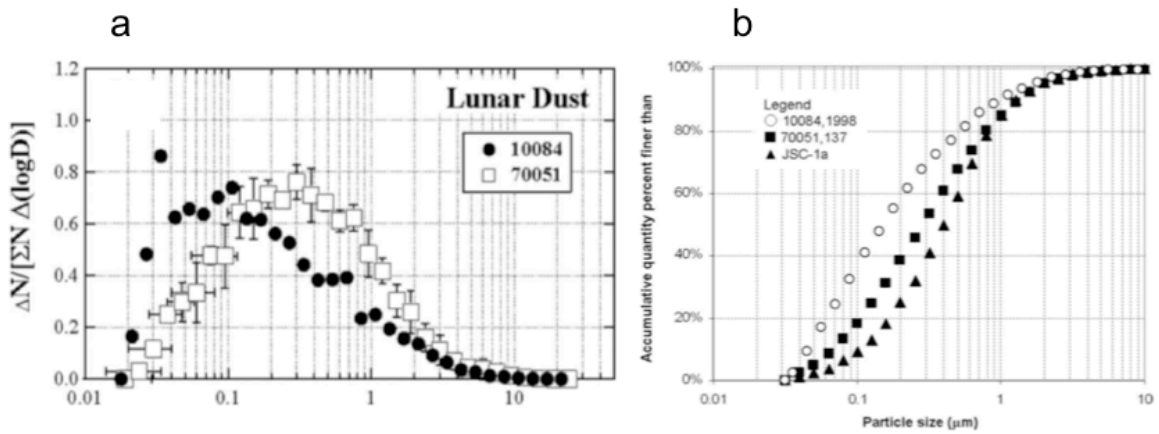

Figure 1.2 *a.* Particle size distribution and *b.* accumulative quantity percent of particles of Apollo 11 lunar dust sample 10084, Apollo 17 lunar dust sample 70051 and lunar dust simulant JSC-1a [5]

In Figure 1.2.a, it can be seen that the particle size distribution of the dust samples of Apollo 11 (10084) and 17 (70051) that show peaks near 100 and 200 nm, respectively. According to Park [5], the dust sample 10084 is the most typical lunar soil. In Figure 1.2.b, it can be seen that it comprises about 40% of particles less than 100 nm and roughly 95% of the particles are less than 2 μm in diameter.

Lunar grains can be classified into five types based on Scanning Electron Microscope (SEM) images of hundreds of particles.

1. *Glass beads:* volcanic beads, or shock-melt, produced during micrometeorite impacts. They can be perfect round spheres, elongated ellipsoids, dumbbells and teardrops. Glass beads are quite common, smooth, rounded (except for some broken teardrops) and can be found in all size ranges. Figure 1.3. *a*, *b*, *c* and *e*.

2. *Vesicular texture:* grains that contain vesicles, of sizes ranging from 0.1 - 4 μm. Vesicular fragments > 10 μm are rarely found and may contain interior bubbles. Broken vesicles result in grains with sharp edges and jagged shapes. They are formed when solar wind volatiles escape during the melting from micrometeorites impacts, producing agglutinates. Figure 1.3. *h*, *i*, *j* and *k*.

3. *Angular shards:* broken glasses with sharp edges as a result of crushing of larger glassy fragments. Figure 1.3. *m* and *o*.

4. *Blocky fragments:* broken rock grains and minerals, which tend to have irregular edges (some due to cleavages) in the minerals. Figure 1.3. *c* and *d*.

5. *Aggregates particles:* small particles loosely attached to each other or to the surface of large particles. It is common on uncleaned samples. Figure 1.3. *g*.

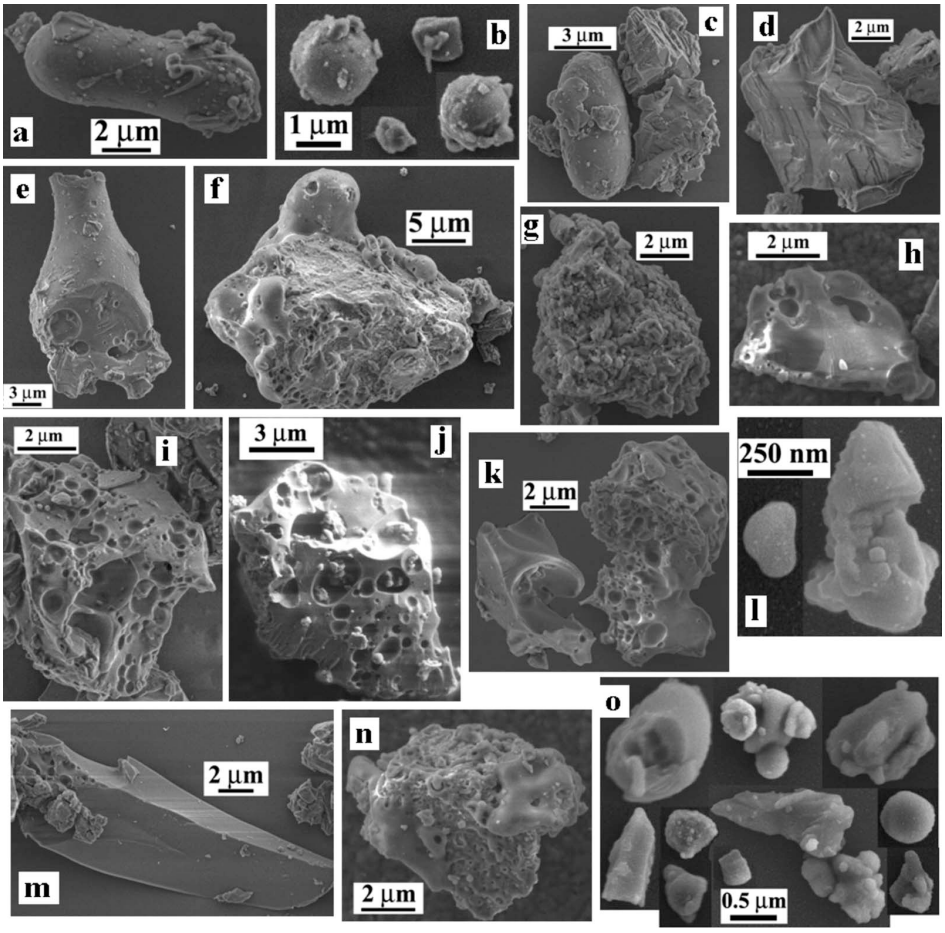

Figure 1.3 Examples of different lunar grains [6]

1.1. Composition

The regolith is composed basically of basaltic components, such as plagioclases (mostly anorthite, olivine and pyroxenes; other minerals, like ilmenite, crystobalite and apatite. Natural metals are also observed forming nanoscale deposits of fully reduced metallic iron (nanophase iron) [7].

Furthermore, as much as 20 wt % of the soil may be glassy material. The relative amounts of these minerals vary somewhat between the two main topographical regions: the maria or *seas* which are rich in Fe, Ti and Mg (mostly in the form of ilmenite, olivine) and the highland regions rich in anorthite (60 wt %) [3].

Table 1.1 Major compositional elements of the two main topographical regions: the Maria **(**Soil 71060, Apollo 17) [7] and the Highlands (Soil 67711, Apollo 16) [8]

Major compositional elements	Maria (wt %)	Highlands (wt %)
SiO_2	40.09	44.20
TiO_2	9.23	0.26
Al_2O_3	10.70	29.40
Cr_2O_3	0.49	-
FeO	17.85	2.96
MnO	0.24	0.06
MgO	9.92	3.86
CaO	10.59	16.30
Na_2O	0.36	0.73
K_2O	0.08	0.11

1.2. Formation

Micrometeorite impacts are responsible for erosion during formation of lunar soil, but there are also other agents, like thermal cycling, creep and solar wind erosion. The lunar surface is exposed to hypervelocity meteorite impacts and thereby larger soil particles are comminuted to finer ones. Silicate glass, formed by some impacts, welds together soil grains into glassy aggregates called agglutinates.

Native iron (Fe^0) in Apollo 11 samples was found. The majority of this Fe^0 in the lunar soil was formed by the auto-reduction of the FeO in silicate melts and vapours, as these were formed by micrometeorite impacts of the silicate minerals in the lunar soil. This effectively caused the FeO in the impact melt to be reduced to elemental Fe^0 that became supersaturated and nucleated homogeneously to produce myriads of nanophase-sized (3-33 nm) Fe^0 particles [1].

1.3. Properties

The Moon has a tenuous atmosphere with an atmospheric pressure of about 10^{-13} kPa, the gravity is approximately 1/6 th of that of the Earth (0.165 g) and the surface temperature varies from 100 K to 395 K, depending on whether it is exposed to sunlight [9].

Moreover, there is no magnetic field; thus high-energy electrons and protons from solar wind and the full spectrum of the sun's electromagnetic radiation reach the lunar surface, with levels of about $2 \cdot 10^6$ rads [9].

Lunar dust can hold charge because it has low electrical conductivity, but it can be increased with surface temperature, Infra-red (IR) light by a factor of 10, and Ultra-Violet (UV) light by ~ 10^6 [10]. Thus, the layer of dust is electrostatically charged, which implies tendency to adhere to surfaces. The strength of dust adhesion to metallic surfaces (i.e. aluminium) is ~ 0.2 - 0.3 kPa/cm^2 and to painted surfaces is ~ 1 kPa/cm^2 [10].

The electrostatic charging of lunar regolith is due to the micrometeorite impacts over billions of years, the solar wind engulfing the moon's surface and the photoionization of the dust particles, as shown in Figure 1.4.

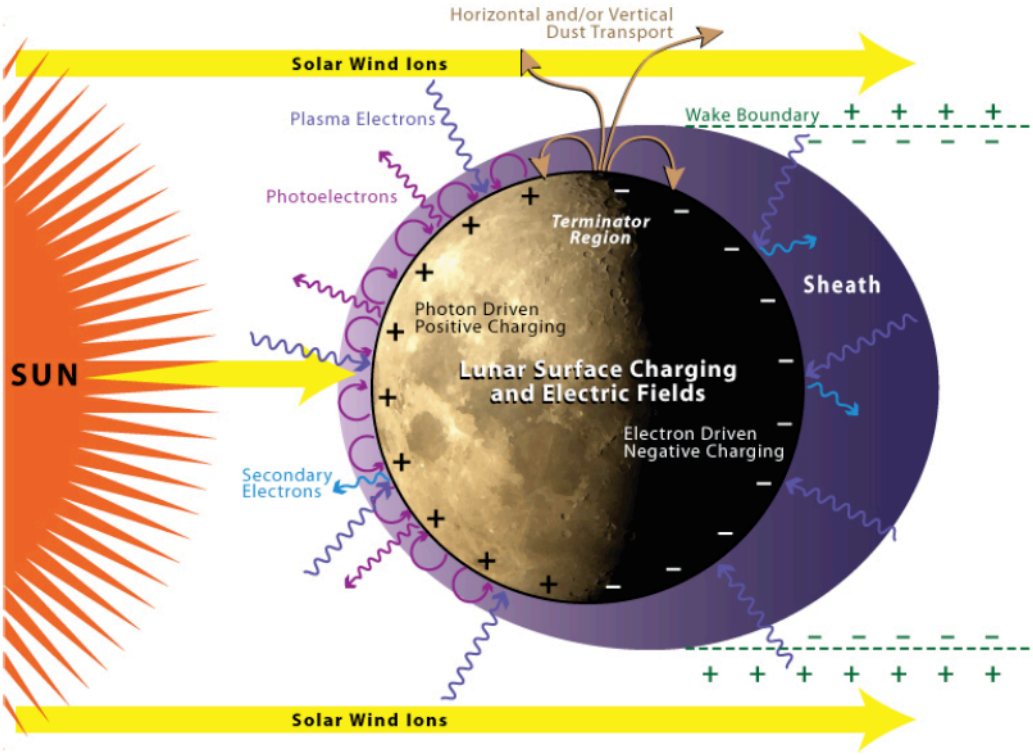

Figure 1.4 Schematic of the lunar surface charging and electric fields [11]

Therefore, dust is positively charged on the dayside where photoemission dominates (with solar wind ions and plasma electrons bombarding the surface, which cause photoelectrons and secondary electrons to be ejected from the surface), and negatively charged on the nightside where collection of solar wind electrons dominates [12].

Besides the electrostatic charge, the finest dust particles (with diameter less than 45 μm) are also magnetic because of the constant bombardment by micrometeorites that form agglutinates which contain native iron [9].

The individual particles on the surface have different charges [4]; contact charging is due to differences in the work functions of particles or mineral grains within particles, and triboelectric charging is due to friction between particles (Individual grains finer than 50 μm can acquire a triboelectric charge of ~ 10^5 electrons [13]).

1.4. Mechanisms of transport

The transport and suspension of particles on the Moon are different from that on the Earth due to the lack of an atmosphere.

Many lunar particles are sprayed out as "secondary ejecta" with each primary meteoroid impact into the lunar surface. The number of these secondary ejecta depends on the size and velocity of the incoming meteoroid, but a single typical hypervelocity meteoroid impacting at 20 km/s may eject 100 to 1000 times its mass in secondary particles, depending on its angle. For example, every square meter of the Moon's surface is impacted by an average of 95 primary meteoroids per year, so roughly 10^{-7} and 10^{-1} g/m^2 per year of material is transported through primary and secondary ejecta, respectively [7].

In 2005 Stubbs [14] presented a dynamic “fountain” model to explain how sub-micron dust is able to reach altitudes of up to ~100 km above the lunar surface, since previous levitation models explain how heavier micron-sized grains behave in close proximity to the surface, but they cannot explain the presence of extremely light grains at high altitudes. However, the dynamic fountain model can explain it relaxing the constraints and assuming that the grains are in constant motion, under the action of dynamic forces.

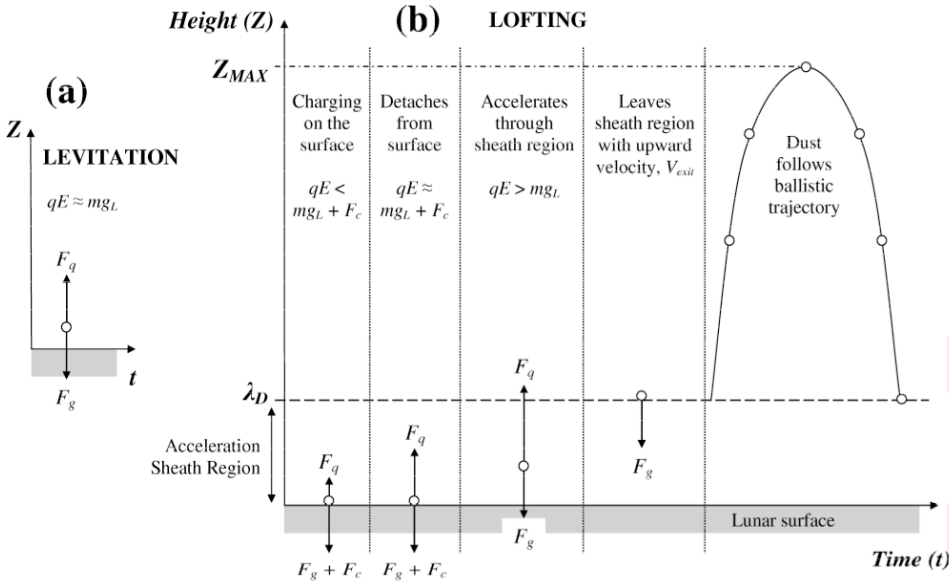

Figure 1.5 Schematic of *a.* The levitation model and *b.* the dynamic fountain model [14]

In the levitation model, dust grains find a point near the surface where the electrostatic (F_q) and gravitational (F_g) forces are about equal and opposite, so they are suspended, as shown in Figure 1.5.a. On the other hand, in the dynamic fountain model, once the dust grains have sufficient charge to leave the lunar surface, they are accelerated upward through a sheath region with a height of the order of the plasma Debye length (λ_D). The smaller dust particles (initially $F_q >> F_g$) leave the sheath region with a large upward velocity (V_{Exit}) and follow a near-parabolic trajectory back toward the lunar surface because of gravity, as shown in Figure 1.5.b.

In the lunar dayside, positive charges build up until the tiniest particles of lunar dust are lifted from meters to kilometres high, the extremely light particles reaching the highest altitudes. They finally fall back toward the surface where it is repeated over and over again [14].

In the night side, electrons in the solar wind flow around the Moon onto the night side charging negatively the lunar dust. According to this model, the dust seems to gain higher voltages, launching them to higher altitudes and speeds, as seen in Figure 1.6.

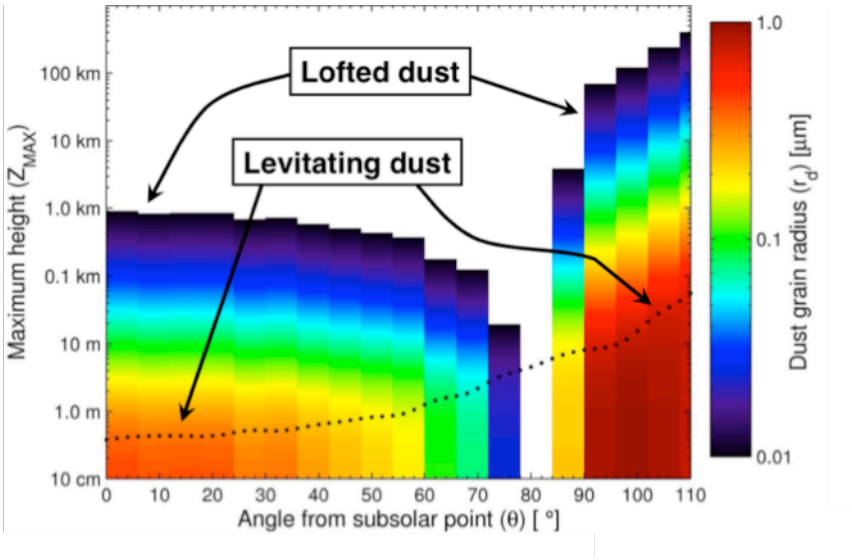

Figure 1.6 Maximum height depending the dust grain radius and angle from subsolar point [14]

The terminator is the boundary between the lit and unlit sides of the Moon and there, there could be significant horizontal electric fields, so dust might be in horizontal transport. On the terminator, there is an electrostatic effect known as "horizon glow", which is a thin, bright streak that traces the horizon caused by the diffraction of light off a low cloud of lunar particles. The charged particles from the sunlit near the terminator hop up and over to the dark side, where some of the photoelectrons have accumulated. The result is a "churning" of soil as the terminator progresses across the Moon, with particles of about 5 μm hopping 3 to 30 cm from the lunar surface. The Horizon Glow, as shown in Figure 1.7, typically extends 2º or 3º on each side of

the sunset line and persists for 90 minutes after local sunset. By this theory, a projected 300 g/m^2 of lunar soil is electrostatically levitated each year [7].

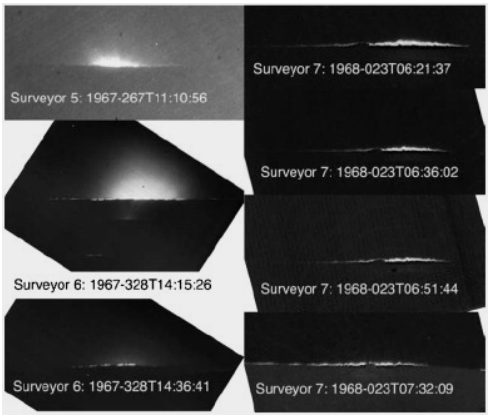

Figure 1.7 Lunar horizon glow observed by the Surveyor 5, 6 and 7 [4]

As explained before, in Figure 1.8.a, it can be seen that the smallest dust grains reach maximum altitudes of about 1 km at the dayside and 100 km in the nightside. And they are lofted to the maximum height on timescales of ~ 30 to ~ 300 seconds, respectively, as shown in Figure 1.8.b. The dust grain travel times to Z_{max} tend toward infinity as grain sizes approach the r_{max} lifting limit. This shows that static dust grain levitation is the limiting case of our dynamic model.

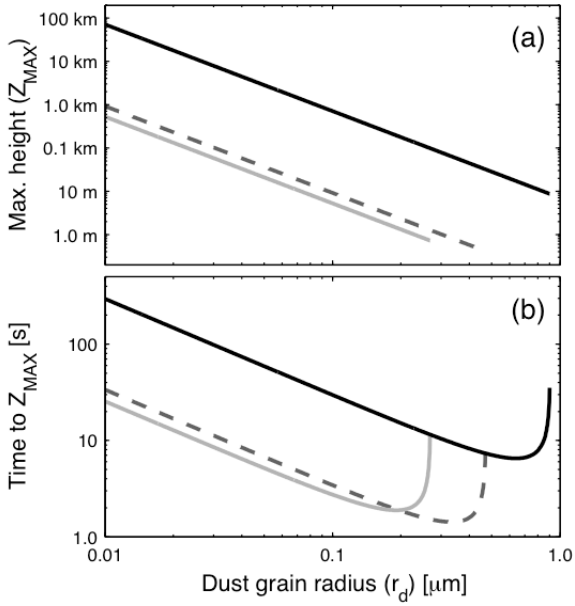

Figure 1.8 Time needed for a lunar dust particle to reach the maximum height depending on the dust grain radius at the subsolar point (dark grey dashed-line), at the terminator (black line) and in an intermediate region (light grey line) [14]

1.5. Hazards

Lunar dust is detrimental to the operation of most mechanical systems and human health, as it can easily levitate and penetrate into mechanical devices, space suits and habitat compartments, causing vision obscuration, false instrument readings, dust coating and contamination, loss of traction, clogging of mechanisms, abrasions, thermal control problems, seal failures, and so on. Besides, it is a threat to humans because it can produce irritation (i.e. nasal issues) and inhalation problems (i.e. severe respiratory diseases like pneumoconiosis) [15].

1.5.1. Photovoltaic Array obscuration

As dust particles are electrically charged they become very adhesive reducing drastically the efficiency of the solar panels and optical elements, such as lenses and telescope mirrors. For instance, the upper portion of the clear filter, positioned over the Surveyor camera lens, had 25% of its surface area covered by dust of about 0.8 μm and 15 μm in size [16]. That caused a marked loss of contrast in relayed pictures, therefore special considerations must be made for solar cells, optical instruments and, in general for systems designed for space applications.

In order to comprehend how much the efficiency of photovoltaic arrays is reduced, Katzan et al. [7] first calculated the probability ***P*** of a point on the surface of a solar array remaining unobscured:

$$P = \left(1 - \frac{\gamma a}{A}\right)^N \tag{1.1}$$

Where γ is the relative transmittance of a lunar particle which is 0.45 of an average particle, ***a*** is the cross-sectional area of the particle, ***A*** is the area of the entire surface, and ***N*** is the number of particles of the same size. Then a substitution is made, ***j***, which is a dummy variable.

$$j = \frac{A}{\gamma a} \tag{1.2}$$

By substitution of equation 1.2 and since ***A*** is much larger than ***a***, the fraction of the surface unoccluded by particles $F_{unoccluded}$ of radius ***R*** becomes:

$$F_{unoccluded} = F_0\left[\left(1 - \frac{1}{j}\right)^j\right]^{\frac{2M\gamma}{\rho hA}} = F_0 \exp\left(\frac{-2M\gamma}{\rho hA}\right) \tag{1.3}$$

Where F_0 is the original area fraction of a surface, M is the mass of all dust particles, ρ is the density (average lunar rock density 3.01 g/cm^3) and h is the particle height (the lunar dust simulant used is MLS-1, which has an average size of 18 μm [7]).

The unoccluded area is directly related to the transmittance of light, to an initial approach. Therefore, the transmission of light through a layer of particles is:

$$\tau_2 = \tau_1 \exp\left(\frac{-2M\gamma}{\rho h A}\right) \tag{1.4}$$

Where τ_2 is the optical transmittance of a clean surface and τ_1 is the optical transmittance of a dust-covered surface.

If all lunar particles were spherical (really only true for about 20% of lunar soil) a 55% reduction would be predicted for 3.5 mg/cm^2 of lunar dust. For particles of higher surface area to volume ratio, the penalty is much greater for the same amount of dust. For example, if all lunar particles were cubic, an accumulation of 3.5 mg/cm^2 would reduce transmittance by 75% [7].

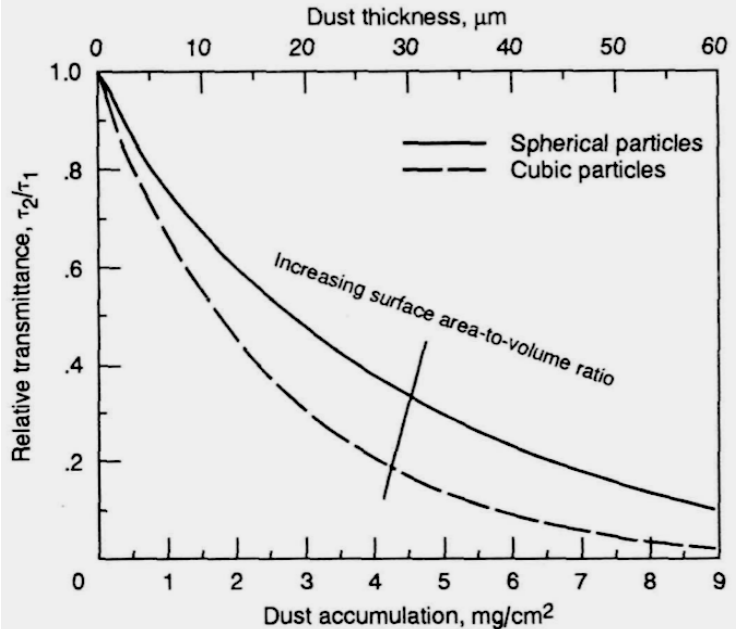

Figure 1.9 Relative transmittance of glass as a function of dust accumulation on its surface. Spherical and cubic particles are compared [7]

It is estimated that 1 mg/cm^2 of lunar soil arrived at the Surveyor III from the landing of the Apollo Landing Module. By the model in Figure 1.9, that amount of dust could reduce transmittance to less than 20% or 30% for spherical and cubic particles, respectively. Similarly, for a dust layer of 10 mg/cm^2, a solar cell would receive less than 20% of its optimal illumination [7].

Hence, due to the high cost of launch per pound of payload the efficiency of these instruments needs to be as high as possible. Causes of degradation of the efficiency include also ultraviolet (UV) light exposure, dust exposure, radiation, plasma sputtering, impact damage, high temperature gradients and contamination. The incorporation of dust mitigation technology can help stop the degradation of the solar panels; however, the additional materials and processes needed for these technologies must not adversely affect the solar panel efficiency.

Chapter 2

ELECTRODYNAMIC SCREEN (EDS)

2.1. State of the art

Masuda in the 70s [17] introduced the concept of electric curtain, which consists in transporting particles by electric wave in motion. Later, in the early 2000s, an electrodynamic dust shield was developed which would evolve to the concept of *electrodynamic screen* [18].

This technology, developed to optimize the efficiency of solar panels used in future space missions on the Moon and Mars, has been shown capable of cleaning dust from various surfaces and prevent its accumulation and enhance the performance of the components [19].

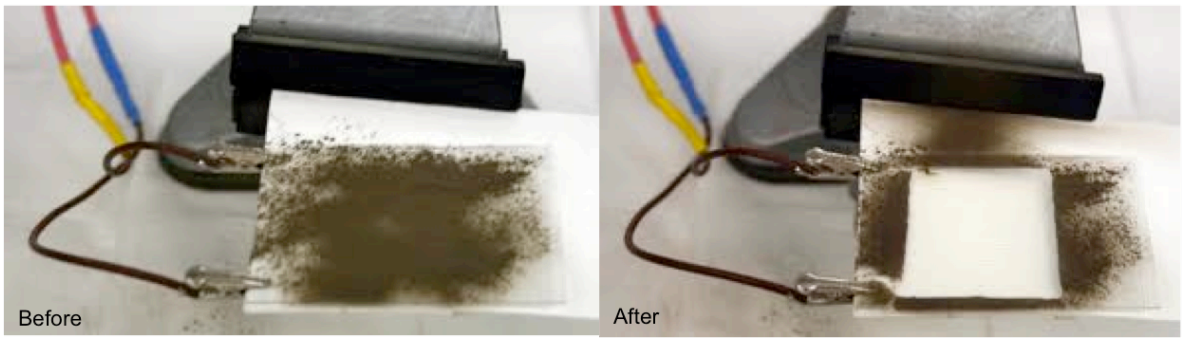

Figure 2.1 A transparent Electrodynamic Dust Shield (EDS) before and after an electric pulse [18]

In 2005 the first patent of Electrodynamic Screen (EDS) was published [20] where the electrodes are embedded in a dielectric transparent film, which is a non-conductive substrate of 50 μm with high electrical resistivity for EDS operation and to protect the electrodes from weathering.

The dielectric layer can be made of polyurethane or fluoropolymer (e.g. ETFE – Ethylene Tetrafluoroethylene), being the later more common because it meets almost all the requirements; over 90% of transparency, UV resistant, excellent contact charging and scratch and moisture resistant.

The electrodes are arranged in parallel rows that cover the entire transparent panel and are made of either metal wires or conducting transparent strips. A thin layer of SiO_2, of 2-5 μm in thickness, coats the electrodes against voltage breakdown, when low frequency and high voltage, and improves adhesion between electrodes and the

substrate. The EDS is placed on a substrate that can be made of borosilicate glass plate, fluoropolymer or PET.

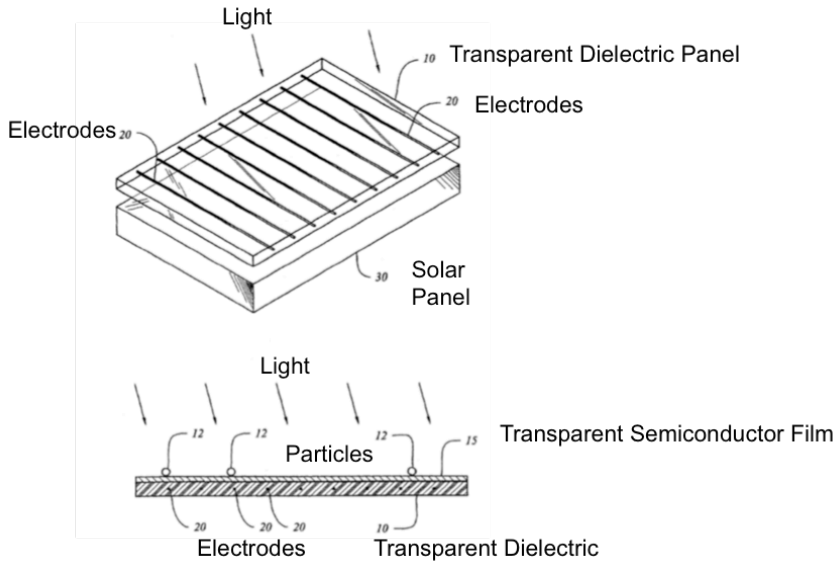

Figure 2.2 Model of an electrodynamic dust shield [20]

As shown in Figure 2.3, the electrodes are connected to a single- or multi-phase AC source fed in turn by the solar cell or by an external source if the EDS is placed in an optical system. The alternating current produced by the solar is continuous before connection to the electrodes; therefore the monitoring unit must convert the direct current to AC. The monitoring unit also controls the intermittent activation of EDS depending on the obscuration of the solar panel.

The panel is coated with an infrared reflective coating to minimize heating of the photovoltaic array, which can result in a reduction of the efficiency.

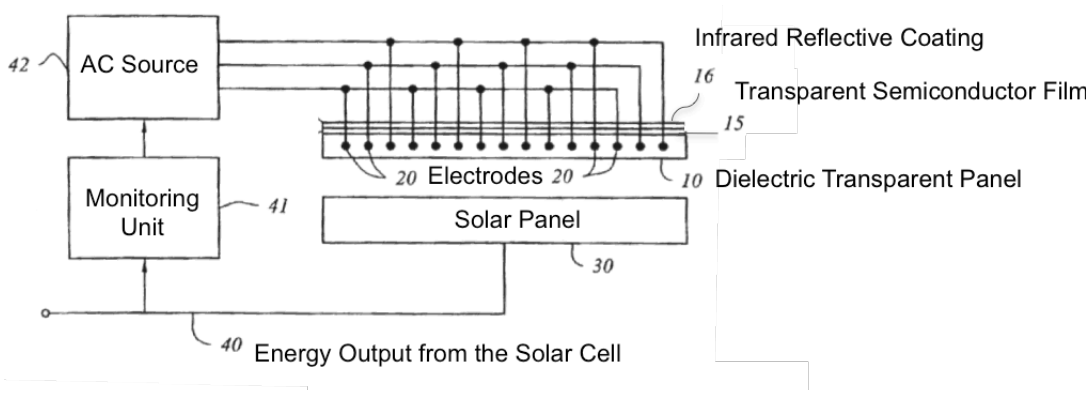

Figure 2.3 Block diagram of the dust shield showing a multi-phase AC source [20]

2.1.1. Basics

Most of the dust carries an electrical charge. Therefore, the production of alternating electric fields, which act through the thin layer of EDS, achieve mobilization and transport of particles deposited as a conveyor belt does. The initially uncharged or very lowly charged particles come also mobilized and transported because as soon as they touch the surface of the shield and collide, they become electrified by triboelectrification.

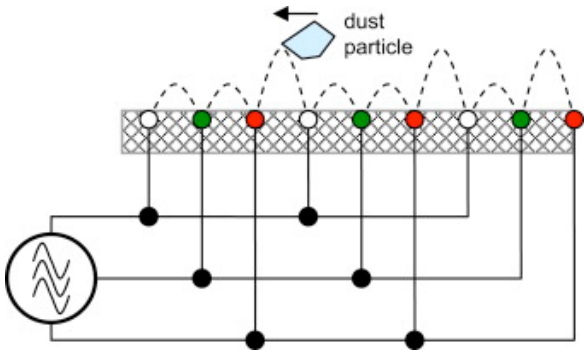

Figure 2.4 Schematic diagram of a multiphase EDS [21]

The triboelectrified particles follow the direction of the wave depending on their polarity. Negatively charged particles will move in one direction, while the positive in the opposite. The EDS acts, in this regard, as a load separator.

2.2. Electric field distribution

In an electric field generated by an electrodynamic screen, the movement of particles can be described by an equation with 6 degrees of freedom [22].

$$m_i\ddot{x}_i = -6\pi\eta R\dot{x}_i + q_iE + F_{image} + F_{dipole} + F_{adhesion} + m_ig, I_i\ddot{\theta}_i = 0 \quad \textbf{(2.1)}$$

Where **x**=(x,y,z), **m** is the mass particle, **η** the viscosity of air, **R** is the radius particle, **q** is the charge of the particle, $\mathbf{F_{image}}$ is the electrostatic force due to a load on the electrodes, $\mathbf{F_{dipole}}$ is the dielectrophoresis force, $\mathbf{F_{adhesion}}$ is the adhesion force, **g** is the gravity acceleration, I is the inertia of the particle, and **E** is the electric field:

$$E = E_0 + E_q = -\nabla\phi + E_q \quad \textbf{(2.2)}$$

Where $\mathbf{E_0}$ is the electric field generated by the AC source and $\mathbf{E_q}$ is the electric field generated by the charged particles.∇

The main force acting on the particle is the *adhesion force*, which is formed by the electrostatic force, the viscous force, capillary force, the van der Waals forces and the gravitational force. In general, as particles get smaller the adhesion force is greater therefore they become harder to remove from a given surface. Thus, the *repulsive force* generated by the application of the electric field has to overcome the adhesion force to move the particles.

The *Coulomb force* [q_i (E_0 + E_q)] applies for charged particles or for those that become charged due to triboelectrification between the dust particles and the screen's surface and the *dielectrophoresis force* applies for both uncharged and charged particles). Both forces induced by non-uniform electric fields are responsible for movement of the particles on the EDS and thus repelled by electrostatic force.

To simplify, it can be said that the magnitude of the electric field and the particle motion will depend mainly on the applied voltage, on the distance between electrodes and on the initial charges of the particles.

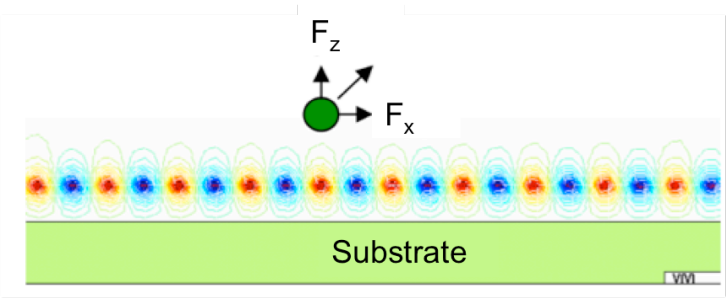

Figure 2.5 Electrical field distributions around the electrodes of the shield [17]

Where $\mathbf{F_x}$ is the transport force and $\mathbf{F_z}$ is the repulsion force.

These forces, $\mathbf{F_x}$ and $\mathbf{F_z}$, are proportional to the voltage applied to the EDS, so the higher the voltage, the greater the movement of the particles.

For what concerns the shape of the electric field has been shown that this becomes uniform along the electrodes. Therefore the field modeling can be simplified to the study of a cross section of the system. Figure 2.6 shows three different configurations of the electrodes in an EDS and the electric field lines for each case.

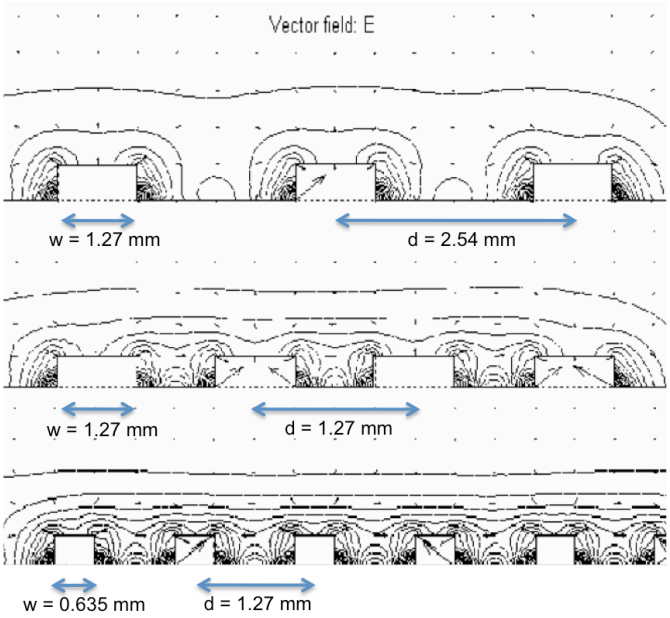

Figure 2.6 Electric field for various EDS electrode geometries in two dimensions [19]

As shown in Figure 2.6, there is a high concentration of electric field lines near the corners of the electrodes and low electric field strength over the center of electrodes. Because of the weak electric field, dust is deposited rather easily in the center of the electrodes while the space between the conductors is cleaned efficiently, because there is no horizontal component to the electric field over the electrode centerline [19].

2.3. Conveyor configuration

The configuration of EDS depends on the number of phases of the AC signal applied. There are different curtain diagrams of one, two and three phases illustrated in Figure 2.7.

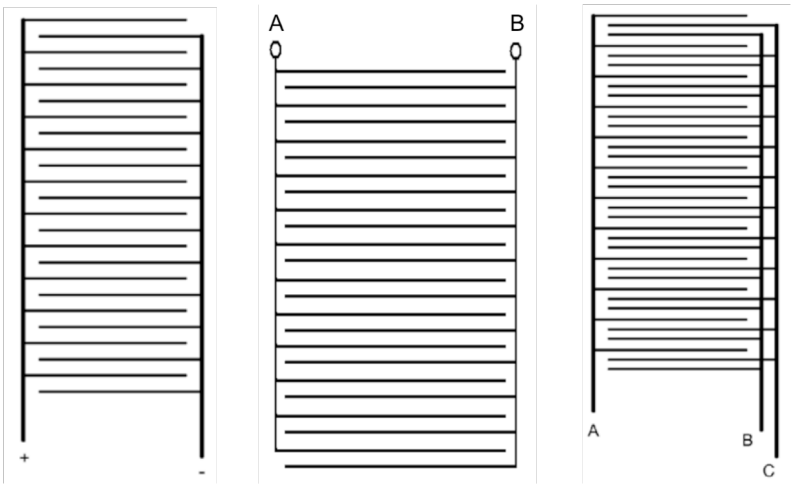

Figure 2.7 Conveyor with one, two or three phases [23]

The multi-phase curtain (three or four stages) generates an electromagnetic wave in non-uniform motion, which more precisely controls the transport of the particles, compared to the case of a monophasic or biphasic curtain [24].

Besides the number of phases of the signal, the structure of the conveyor system changes also depending on the configuration of the electrodes. This can be parallel, square vortical (for solar panels and mirrors) or circular vortical (for optical lens) [22], as shown in Figure 2.8.

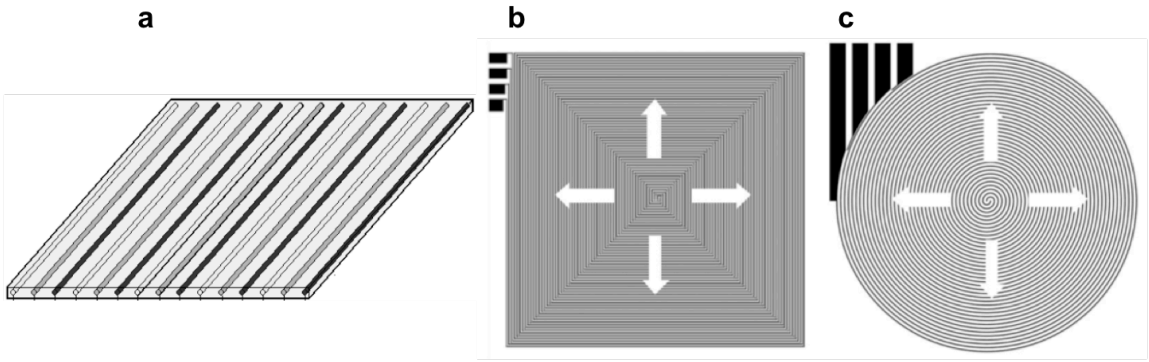

Figure 2.8 Conveyors with different electrodes configurations *a.* parallel [25], *b.* square vortical and *c.* circular vortical [22]. The arrows in *b* and *c* indicate the direction of particle motion when activating the EDS

The configuration with parallel electrodes is the simplest to construct, although the connections between the electrodes and the power source have to be three dimensional to avoid intersections between phases. However, in the vortical configuration the implementation phase is more complex while the connection between the electrodes and the power source can be two-dimensional.

2.4. Electrodes design

A more uniform electric field distribution implies a better cleaning of the dust layer, thus the cross-sectional shape for the electrodes has an important role. They usually are square or rectangular, but triangular or pyramidal cross-sectional shape is believed to provide the most desirable surface distribution of electric field. However, this section is difficult to produce, so hemispherical shape may be an optimum choice [23].

Another important aspect to consider when designing the electrodes is the materials with which the electrodes are going to be produced. The main characteristics of the materials must be high electrical conductivity and optical transparency and the possibility of developing in thin layers. The nanoparticles that constitute the Transparent Conducting Films (TCFs) meet these requirements.

The TCFs are already used in photovoltaic cells for increasing the transmissivity of the solar panel, acting as a window for light to pass through the underlying asset material (where the load is generated) and as an ohmic contact to the output of the load from the PV system [26].

In general, electrical materials used in photovoltaic applications use materials with greater than 80% transmittance of incident light, electric conductivity greater than 10^3 S/cm for the efficient cargo transportation and preferably with a very low surface resistivity (less than 100 Ω/sq). Transparent materials have *bandgaps,* with energies corresponding to the wavelengths shorter than the visible range (380 nm to 750 nm). Thus, photons with energy below this band are not absorbed by these materials and are traversed by visible light. However, in the applications of these conductive films in solar cells can require a band range greater than 380 nm to avoid unwanted absorption of the solar spectra [27].

The TCFs applicable to photovoltaic cells can be composed of inorganic and organic materials. The inorganic films, which typically are composed of a layer of TCO (Transparent Conductive Oxide), usually in the form of Indium-doped Tin Oxide (ITO), doped Fluorine-doped Tin Oxide (FTO), and doped zinc oxide. While the organic films use carbon nanotubes networks and graphene.

Currently TCO used are *n-type* conductors. The main advantage of a transparent conductive oxide is its good electrical conductivity that contrasts with its main disadvantage; fragility and tendency to break due to fatigue. At present, the industrial transparent conductive oxide most widely used is ITO. However alternatives are considered since indium is very expensive, like AZO (Aluminium-doped Zinc Oxide).

Doped metal oxides used as transparent conductive layers for photovoltaic devices are typically performed on a glass substrate. This glass substrate, as well as providing support for the oxide, has the added advantage of blocking the majority of the infrared wavelengths greater than 2 μm for most of the silicates, and convert them into heat in the glass layer. This in turn helps to keep the temperature of the active region of the solar cell, the performance of which decreases when heated.

The following table summarizes the main advantages and disadvantages of each material.

Table 2.1 Main advantages and disadvantages of ITO, AZO and CNT

Transparent Conductive Films (TCF)	Advantages	Disadvantages
Indium-doped Tin Oxide ITO (In_2O_3/Sn)	Good electrical and optical properties. Ease of manufacture.	Indium is rare and expensive ($680/kg). Brittle.
Aluminum-doped Zinc Oxide AZO (ZnO/Al)	Non-toxic. Aluminium and Zinc are common and cheap. Low electrical resistivity and good optical transmittance.	Lower electrical conductivity than ITO.
Carbon Nanotube (CNT)	Flexible and UV resistant. High optical transmittance and conductivity. Ease of manufacture.	Higher sheet resistance than ITO.

2.4.1. ITO

The Indium Tin Oxide (ITO) is a solid solution of indium oxide (In_2O_3) and tin oxide (SnO_2), typically in weight percentage of about 90% and 10%, respectively. It has good electrical properties, ease of manufacture and reflects radiation in the infrared region as a normal metal.

The main feature of ITO is a combination of good electrical conductivity of 10^3 – 10^4 S/cm and optical transparency over 90%. This material also provides a sheet resistivity greater than 100 Ω/sq, but there are technologies capable of reduce it to less than 100 Ω/sq [23].

However, it has the disadvantage of being expensive. Due to the limited availability of indium and its growing market demand, its cost has increased significantly; 680 $/kg of indium in 2014, as seen in Figure 2.9.

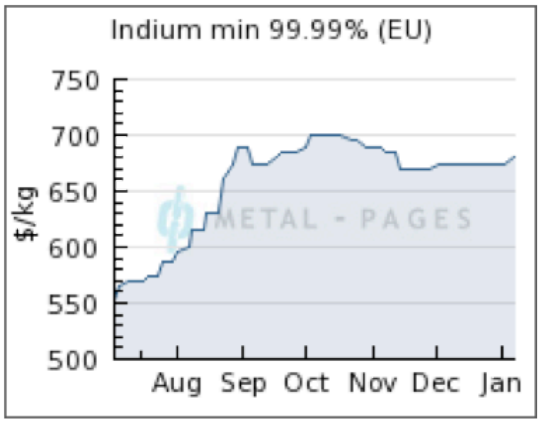

Figure 2.9 Indium prices between July 2013 and January 2014 [28]

Other disadvantages are that the ITO thin films are fragile and can present problems such as lattice mismatch, limitations of stress-strain and degradation over time when it is subjected to mechanical stress. The fragility and limited flexibility of the layers of ITO and the high cost of deposition techniques, which require high temperatures and high vacuum levels, are forcing to look for other alternatives.

2.4.2. AZO

Currently, a good alternative to ITO is Aluminum-doped Zinc Oxide (AZO), which is composed of basic, inexpensive, non-toxic and abundant materials for applications of thin transparent electrodes. Moreover, when are incorporated elements from group III of the periodic table (B, Al, Ga and In), particularly Al, the zinc oxide becomes a p-type material with improved electrical and optical properties; transmittance in the visible region over 90% [23] and lower sheet resistance than ITO, as shown in Figure 2.10. This improvement is due to the increase in concentration and mobility of carriers.

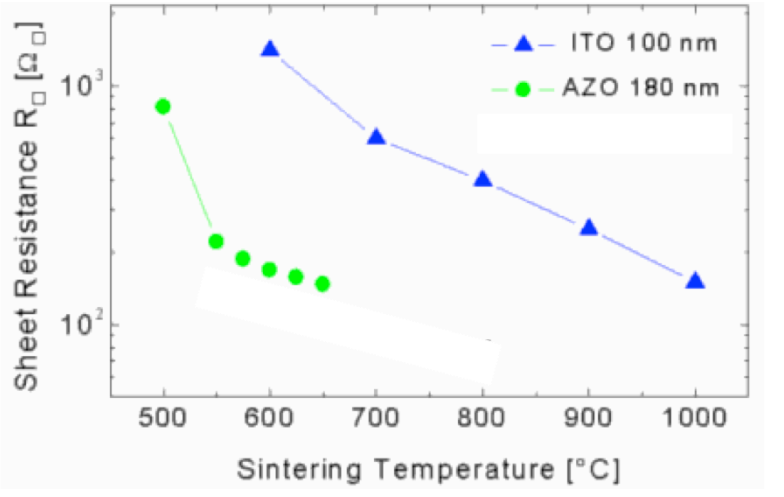

Figure 2.10 Sheet resistance of ITO and AZO depending on the sintering function [29]

Figure 2.11 shows the evolution of zinc price in the second semester of 2013. And comparing with indium (680 USD/kg), there is a significant difference in price since zinc costs 2.03 USD/kg.

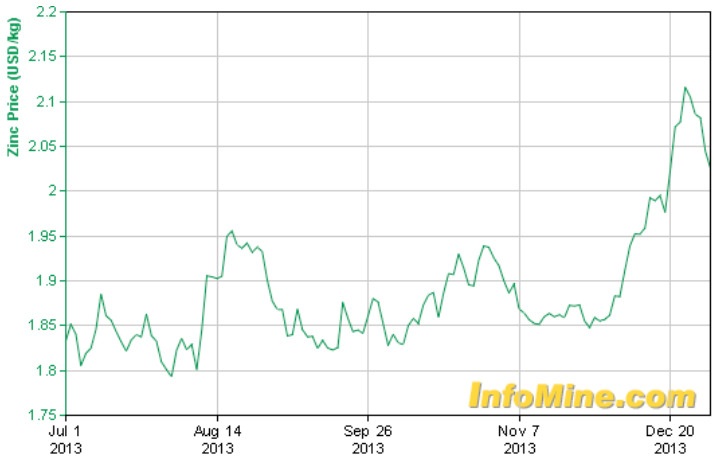

Figure 2.11 Zinc price between July 2013 and January 2014 [30]

2.4.3. CNT

Carbon nanotubes (CNT) are under research because of their outstanding characteristics; extremely high conductivity, high aspect ratio, high transmittance, superior flexibility, UV resistant, good adhesion to the substrate and environmental stability.

They are also made of inexpensive materials and their deposition costs are economical, what makes CNT a good candidate to replace ITO. Nevertheless, its sheet resistance is quite high 1000 Ω/sq, which can be reduced using super-aligned carbon nanotubes (SACNT), acquiring a sheet resistance of 200 Ω/sq at a transmittance of 85 % [31]. This sheet resistance is not adequate enough, thus it needs to be solved.

2.5. Technology to deposit electrodes on the dielectric

There are different techniques for printing electrodes on the dielectric film of an electrodynamic screen [23].

Thin films of ITO and AZO are commonly deposited using Chemical Vapor Deposition (CVD), Magnetron Sputtering or e-beam deposition methods. They all need high vacuum, which is expensive. Besides thin AZO films can be also deposited using sol-gel process, which still requires heat treatment under vacuum.

Thin films of CNT are deposited using CVD, screen-printing or spray painting.

Photolithography can be used for making masters with the defined configuration.

Chapter 3

MODELING

3.1. Optimizing the configuration of an EDS

In order to properly configure the electrodynamic screen, it is considered appropriate to assess the conditions that have led to a better dust removal efficiency.

In this sense, the results of experiments conducted to date on the Clearing Factor (CF) or Dust Removal Efficiency (DRE) will be analyzed to determine which parameters and to what extent they affect the efficiency of dust removal in an EDS. Thus, the characteristics of the EDS will be defined.

Removal efficiency is measured by calculating the CF [17]. It represents the percentage of dust, which has been removed due to the activation of the EDS, in comparison to the mass of dust initially deposited on the EDS.

$$CF = \frac{m_i - m_f}{m_f} \cdot 100 \qquad \textbf{(3.1)}$$

Where $\mathbf{m_i}$ is the mass of dust deposited and $\mathbf{m_f}$ is the mass of dust removed from the EDS.

The Clearing Factor decreases by increasing the initial deposition of dust because the force applied by the electric field is insufficient to move the mass of the particles of the dust topcoat. Therefore, the EDS works efficiently with a fine layer of dust closest to the surface.

3.1.1. Main parameters affecting the Clearing Factor (CF)

The main parameters that influence the CF are the amplitude, waveform and frequency of the AC signal, which feeds the EDS.

The particles are better removed with higher voltages. At low frequencies, the EDS works better with dust particles already deposited, while at high frequencies, particles do not deposit almost at all. Thus, according to Figure 3.1, the optimal operation range is between 6 and 8 KV for the voltage and between 5 and 15 Hz for the frequency [17].

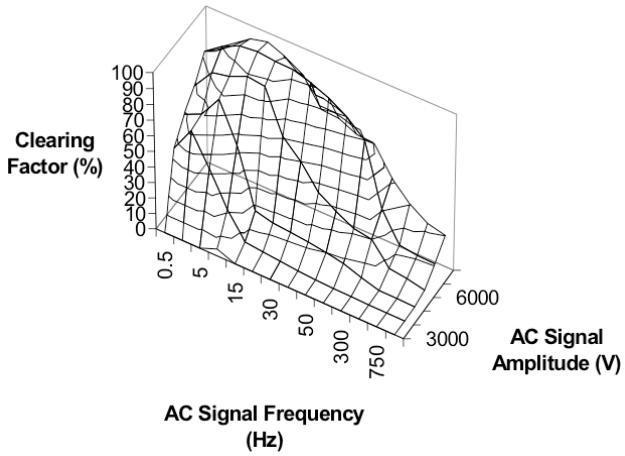

Figure 3.1 Influence of the amplitude and frequency of the AC signal on the Clearing Factor [17]

Regarding the shape of the signal, more particles are removed when the gradient of signal amplitude growth is larger. Therefore, triangular waves behave worse than sinusoidal or rectangular waves, as seen in Figure 3.2.a. The pulsed signal has better efficiency than rectangular or sinusoidal waves because for very short periods, the remaining forces are extremely intense (Figure 3.2.b).

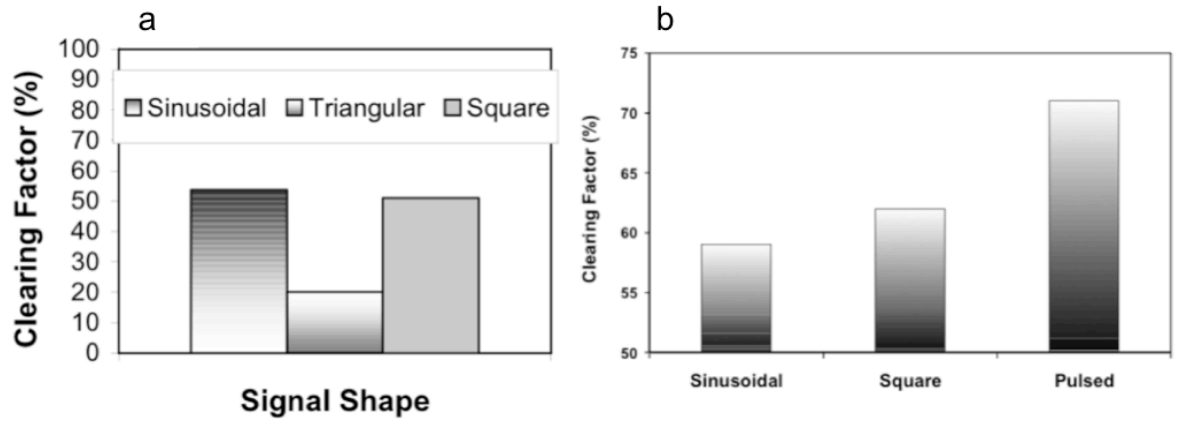

Figure 3.2 The Clearing Factor as a function of the signal shape: *a.* comparison of sinusoidal, triangular and square shapes [17] and *b.* comparison of sinusoial, square and pulsed shapes [32]

Other parameters that influence the CF are the distance between the electrodes, the charges of the particles and their diameter.

Table 3.1 summarizes the results of a test on dust removal efficiency of an EDS under different conditions. Johnson et al. [19] tested two different dust types: one with a more fine-grained and another coarser. The experiment was carried out well without charging the particles and with tribocharged particles. Furthermore, the

configuration of the electrodes, distance between them, was varied to compare the results.

If the particles are tribocharged before they are deposited and there is less distance between the electrodes (d_1 = 1.27 mm), the percentage of removed particles is greater than in the case where the electrodes are placed at greater distances. This agrees because the electrostatic forces of the particles increase.

Table 3.1 Dust removal efficiency depending on their charge and size [19]

Dust removal efficiency		Distance between eletrodes	
		d_1 = 1.27 mm	d_2 = 2.54 mm
Not tribocharged dust	Fine dust	77.3 %	44.7 %
	Coarse dust	47.1 %	28.1 %
Tribocharged dust	Fine dust	85.9 %	40.9 %
	Coarse dust	70.2 %	23.1 %

The results observed in Figure 3.3 shows that the dust removal efficiency is virtually the same for neutral, positive or negative particles. However the dust that is more highly charged is removed faster from the screen since the low charged or neutral particles need to gain charge through triboelectrification [32].

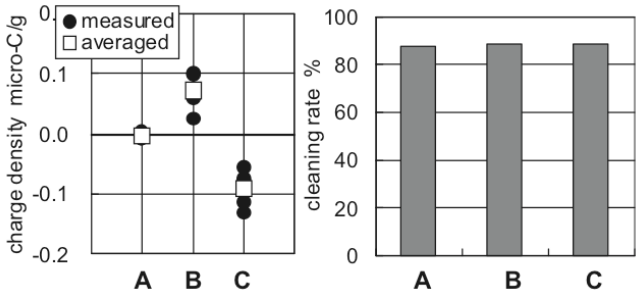

Figure 3.3 Cleaning efficiency of: *a.* Uncharged, *b.* Positively charged and *c.* Negatively charged dust [22]

The diameter of the particles also affects the efficiency of elimination since it increases with increasing particle diameter [22]. This depends on the fact that the forces of adhesion to the surface of the screen are directly proportional to the diameter of the particles. In this respect, the particles of smaller diameter are more difficult to mobilize as seen in Figure 3.4.

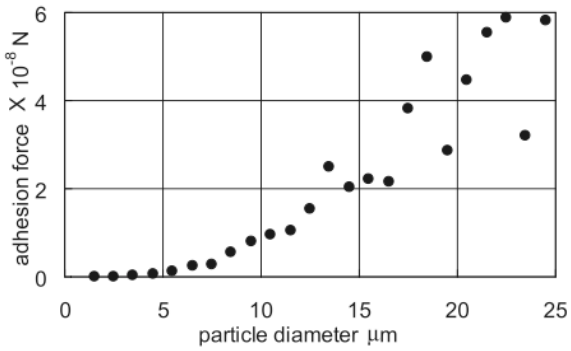

Figure 3.4 Measured adhesion force with respect to particle diameter [22]

3.2. EDS Configuration

As seen in the previous section, there are different parameters affecting the correct operation of the EDS, therefore, it is important to properly define the system configuration.

For this project, we have considered a three-phase electrodynamic screen with square vortical and circular vortical configuration for solar panels and optical lens, respectively. Although parallel configuration is easier to perform it has been taken into account the purpose for which the EDS is designed.

Three different electrode materials are evaluated: ITO which is the most common but very expensive, AZO which has similar characteristics to ITO and is besides affordable, and CNT which has exceptional features but it is still not solved its high sheet resistance. In order to ascertain which material delivers better performance, all three should be tested.

It is also important to define the width **w** of the electrodes and the distance **d** between them because they affect the movement of the particles and therefore the removal efficiency. There are different conditions that must be taken into account:

- The particle diameter cannot be greater than 3.5 times the distance between the electrodes, otherwise the Coulomb force between the particles and the electrodes is canceled and then, there is no transport of particles [22].

- The ratio of the electrode width to the inter-electrode spacing (center-to center) should not be greater than 10:100 to ensure minimal loss of transmission of solar radiation by the EDS placed on the top of the solar panel [23].

- The width of the electrode should be comprised between 50 μm and 100 μm depending on the conductivity of the electrode material and the distance between electrodes in the range of 100 μm to 1000 μm depending upon the size distribution of the dust particles involved. A compromise between optical

transmittance and surface cleaning of dust is needed, because smaller electrode width and shorter inter-electrode spacing are good for fine particles but if the number of electrodes per surface is increased, it causes obscuration. Hence to ensure a cost-effective compromise between dust removal efficiency and transmission efficiency is preferable to have an inter-electrode spacing of 500 μm to 750 μm [23].

In Table 3.2 are listed the chosen values for the initial configuration of the conveyor.

Table 3.2 Initial values for the configuration of the conveyor

Distance between electrodes	d	500 – 750 μm
Width of electrodes	w	50 – 100 μm
Transparent dielectric thickness	h_d	50 μm
Thickness of electrodes	h_e	20 μm

The thickness of the transparent dielectric must be approximately 50 μm to provide the necessary mechanical support, to protect from weathering, and at the same time allow the electric field to propagate from the electrodes to the surface of the shield to remove the deposited dust particles.

Finally, the AC signal must be comprised in the range of values given in Table 3.3 to ensure the maximum efficiency of the electrodynamic screen.

Table 3.3 Initial values for the configuration of the AC signal

Voltage	6 – 8 kV
Frequency	5 – 15 Hz
Wave shape	Pulsed

Chapter 4

CRITICAL ASSESSMENT OF DUST MINIMIZATION EFFECTS IN PV CELLS AND OPTICS

4.1. Solar panels

Solar panels should be ideally placed in areas of constant illumination, that it is to say, in Peaks of Eternal Light (PEL) [33]. However, there are no PELs on the Moon but still there are some places in the poles with significantly more light than the typical 14 days. This occurs because the Moon's spin axis is nearly perpendicular to the ecliptic plane, tilted at ~1.5º. Therefore the lunar Polar Regions experience unusual illumination conditions.

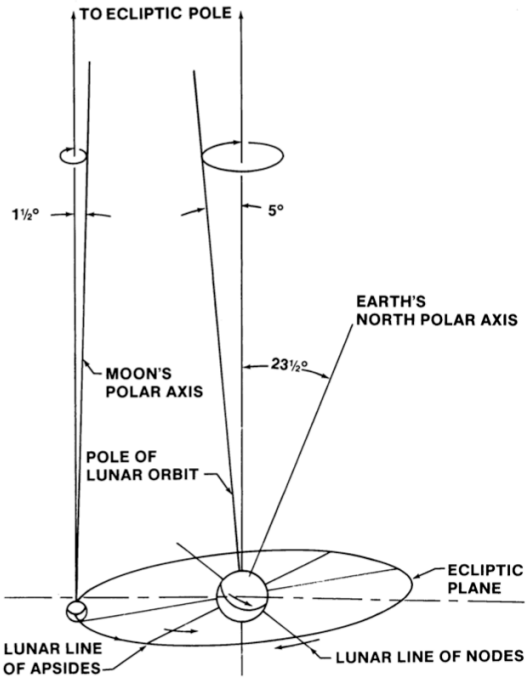

Figure 4.1 Motion of the Earth and the Moon [33]

A National Astronomical Observatory of Japan (NAOJ) team estimated the sunlit conditions of the lunar Polar Regions with the lunar orbiter KAGUYA (SELENE) [34]. The result shows that most continuously lit surfaces are 89% for north and 86% for south, 324 and 314 days of sunlight a year, respectively.

In the Lunar North Pole, The best spot to settle is on the northern rim of Peary crater because of its illumination of 89%. It is located at 88.6ºN 33ºE with 73 km in diameter.

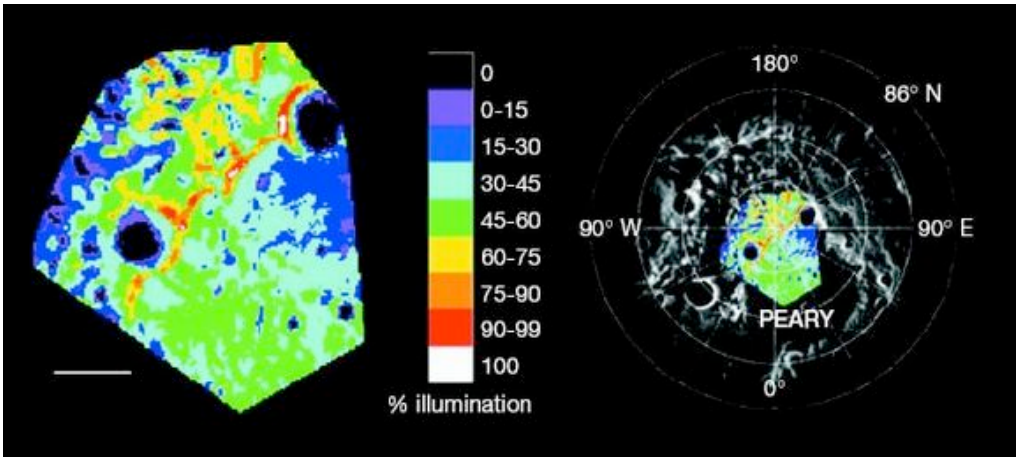

Figure 4.2 Illumination conditions in Peary crater (Lunar North Pole) [35]

In the South Pole, there are also six points found by Bussey [36] shown in Figure 4.2:

- On the rim of Shackleton crater (A: 89.68ºS 166ºW).
- On a ridge close to Shackleton crater (B: 89.44ºS 141.8ºW).
- On the rim of De Gerlache crater (C: 88.71ºS 68.7ºW).
- On a small ridge emanating along the 120ºE longitude line from the rim of Shackleton crater (D: 99.79ºS 124.5ºE).
- Two points on Malapert Mountain (M1: 86.04ºS 2.7ªE and M2: 86ºS 2.9ºW).

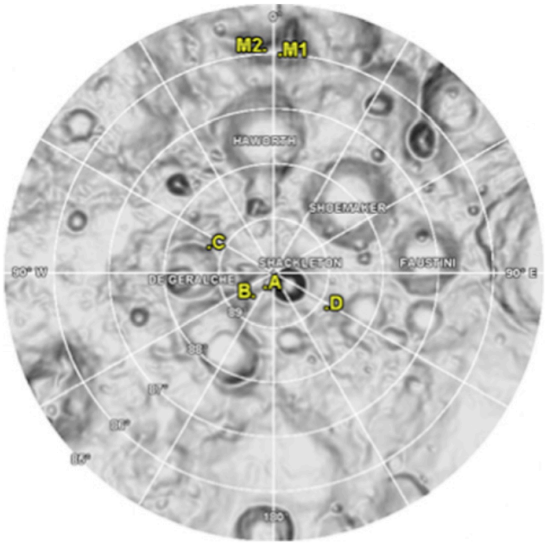

Figure 4.3 Areas identified with the most illumination from 85ºS to the Lunar South Pole [36]

Points A, B, C and D are illuminated for more than 80% of the year, while M1 and M2 more than 70%.

Points A and B together are illuminated for over 8 continuous months and more than 94% of the time, because they are complementary, thus when one is dark, the other is often illuminated. Point B has an annual mean illumination of 82% and receives constant illumination for more than 4.5 continuous months. During the 8-month period centered in the mid-summer, there are short eclipses (between 12 to 24h).

Point C has maximum eclipse of approximately 6 days. Point D is the most illuminated point with an annual mean illumination of 86% and receives constant illumination for longer than 5 continuous months centered on mid-summer. There is an eclipse of approximately 2 days during a 7-month period, when the Sun comes from 285ºW. The longest eclipse for 2020 will last around 11.5 days during mid-winter.

Points M1 and M2 have less illumination than the others, just 74%, in spite of that, they offer continuous line of sight with the Earth.

In this section it has been seen what places offer better illumination conditions to place instrumentation that may be possible to power exclusively with solar energy.

Nevertheless, since the Sun and Earth is always near the horizon at the lunar poles, the terminator is always present in the Polar Regions as well as the Horizon Glow, where dust particles of about 5 μm hopping 3 to 30 cm from the lunar surface.

Moreover, on these peaks in the polar regions where Sun never sets the lunar dust can reach at maximum altitudes up to 1 km with dust grains ranging from 0.1 μm to the smallest ones. But according to the dust fountain model, almost all-levitating dust is under 2 m height in the illuminated areas, as seen in section 1.4. Therefore solar

panels could be better placed at a minimum height of 2 m in order to avoid having to activate the electrodynamic screen so often and, in turn, to reduce the size distribution of dust that may accumulate on the top of the EDS, since most of the particles with diameter greater than 1 or 2 μm will be levitating or lofting under the solar panel.

4.2. Optics

4.2.1. Astronomy from the Moon

The atmosphere of the Earth introduces turbulence and aberrations in the observations and also absorbs most of the incoming radiation. Numerous astronomical events show different signatures along the entire spectrum so as to access the whole electromagnetic spectrum, the observations must be made away from the Earth's atmosphere and magnetic shield [37].

The environment of the Moon offers great advantages to observatories with respect to the Earth's and besides no human presence on the Moon also makes it more astronomically appealing.

The lack of atmosphere of the Moon would results in less investment on costly adaptive optics technology, all wavelengths would be available (from gamma to long radio waves), astronomical instrumentation would not suffer any degradation due to atmospheric erosion, and the resolution it can be achieved is limited only by manufacturing and theoretical restrictions (diffraction limit).

During the day, on Earth, it is not possible to make observations, but the Moon's days (about 14 Earth days) allows for nonstop astronomy due to its dark sky. Furthermore, the Moon offers a more seismic stable platform and only meteoritic impacts perturb lunar quietness enabling the use of simple, low-cost telescope bases [38]. The low lunar gravity also allows making larger, lighter and cheaper structures.

The Moon has no human presence or light pollution. Hence, the farside of the Moon is the cleanest place in the Solar System, as the Moon itself blocks all the Radio Frequency Interferences (RFI is the radio noise sent out by humans on the Earth) making an ideal site for radio astronomy. However the neraside also offers an improvement inasmusch as the RFI is reduced in $1/r^2$ from that on the Earth [37].

Other advantages are no atmospheric scattering, slow rotation, landforms and proximity the Earth (1.3 light-seconds) among others.

Although the Moon also has some drawbacks for astronomical facilities, like micrometeorites, cosmic and solar radiation can slowly damage instruments, very marked changes in temperature as large as 350 ºC [38], and definitely lunar dust would interfere with the telescope operation.

Table 4.1 Advantages and drawbacks of the lunar environment [39]

Lunar Feature	Advantages	Disadvantages
No atmosphere	• Access to all wavelengths. • No atmospheric distortion of images. • No wind loading of telescopes.	• No protection from cosmic rays. • No moderation of thermal effects.
No ionosphere	• No long-wave radio cutoff.	• Line-of-sight transmission.
Size	• Large, disconnected structures can be built. • Momentum from pointed telescopes is absorbed. • Seismically quiet compared to the Earth.	
Solid Surface	• Radiation and thermal shielding. • Raw construction materials.	• Possible dust contamination.
Lunar Gravity	• Lightweight structures possible.	• Telescopes require support.
Slow, Synchronous Rotation	• Two weeks of thermal stability. • Long integration times. • Farside isolated from terrestrial interference.	• 300 K diurnal temperature change. • Very slow aperture synthesis. • No solar power at night.
Distance from the Earth	• Long baseline for radio interferometry.	• Expensive transportation.
Human Presence	• Construction, operation, repair, refurbishment.	• Expense, safety, requirements, environmental degradation.

4.2.2. Optics

No single site is best for all uses because it depends on the purpose: visibility of the Earth, the Sun and the celestial sphere or shielding from the Earth and the Sun. So site evaluation criteria apply to terrain, other local aspects of the environment and celestial accessibility.

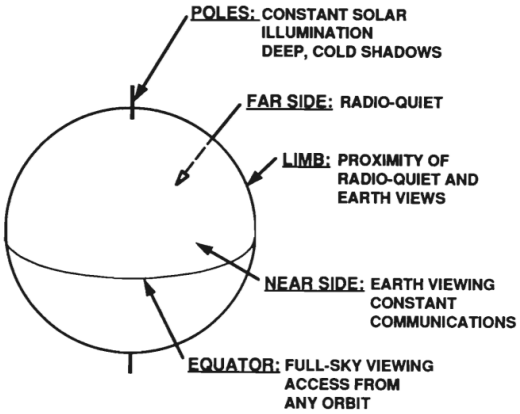

Figure 4.4 Suitable sites on the Moon to place an observatory depending on different purposes [40]

Equatorial locations offer nearly all-sky views for astronomy, most of the farside offers radio isolation, and high crater rims and peaks near both poles offer near-constant sunlight for power generation and permanently shadowed areas at cryogenic temperatures.

Equatorial and polar sites are favored for their near-constant accessibility, slopes offer favored illumination and shadowing, while craters offer natural depressions. Near the equator, cooling is more difficult, but near the pole of about 70º, some craters never receive direct sunlight and their walls provide thermal shielding, allowing cryogenic temperatures (about 30 K) for infrared astronomy and other instruments which need to be as cold as possible, for example liquid-mirror telescope, X-ray and gamma ray astronomy [40].

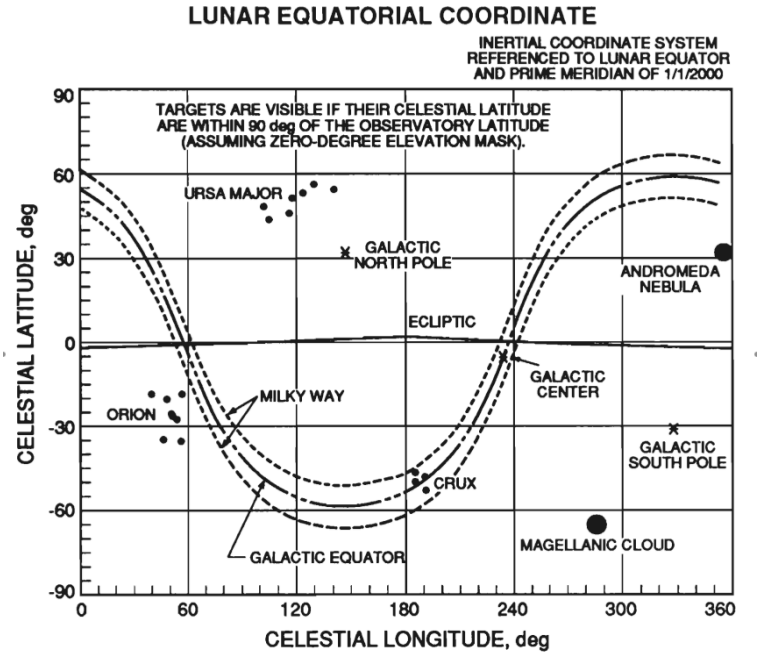

Figure 4.5 View of the sky referenced to lunar equator [40]

Half the sky cannot be seen from either pole, but from near the equator almost all the sky is available at some time during a month [40], as shown in Figure 4.4. However, it is difficult to know how much area of sky is not visible as a function of latitude, thus there is not a single criterion available, as seen in Figure 4.5.

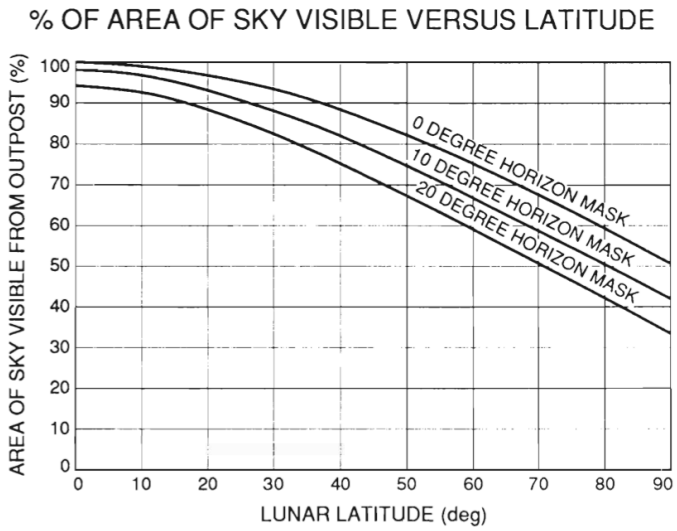

Figure 4.6 Fraction of the sky visible as a function of lunar latitude. Horizon masks refer to the minimum acceptable elevation above the ideal horizon at which observations can be made. [40]

Depending on the number of targets that we want to observe, the location of the telescope can be crucial, because if we just want to study one or few targets, the location of the telescope is very important not to compromise the investigation. In the other hand, if there are many targets, the location of the telescope can be wherever from that any moderate-sized area of the sky is accessible, thus the study may still be performed. However, in some cases the instrument sensitivity and/or aperture can be increased resulting in more target objects becoming available [40].

From a polar site, objects in the sky do not rise or set, but rather just circle around the pole. Therefore interferometric imaging is much enhanced near the equator and at a few hundred kilometres around onto the far side of the Moon, so that the instrument will be protected from natural and man-made radio noise.

For other experiments that need communication with the Earth, the near side sitting is preferable even if the Earth is a bright source of visible light and thermal infrared. In order to reduce these interferences, the telescope can be placed near the limb or near the sub-Earth point where the Earth appears near the horizon or near the zenith, respectively.

In conclusion, the telescope set up is very wide, hence the minimum height to avoid the maximum percentage of dust is very complex to estimate. Besides, for example, the cryogenic telescopes need to be in deep and shadowed craters, where according

to the dust fountain model lunar dust can reach heights from 10 to 100 m, consequently both requirements cannot be met.

Nevertheless, telescope should be better placed at an altitude similar to the solar panels, approximately 1 or 2 m, to avoid the Horizon Glow, where dust particles of about 5 μm hop between 3 and 30 cm from the lunar surface, and to avoid the largest lunar dust particles to interfere on the optics.

4.2.2.1. Shadowed regions

As seen in the section 4.1, in the lunar poles there are places with exceptional illumination conditions, but at the same time portions of the interiors of some craters near the poles are deep enough to ensure that they never see the Sun.

In the North Pole, Bussey [41] mapped 832 craters, with a total surface of 12,500 km^2, from where 7,500 km^2 are in permanent shadow. Some craters like Lovelace E (82.1ºN 94º W and 23 km in diameter), Rozhdestvensky K (82.7ºN 145ºW and 42 km in diameter) and Rozhdestvensky U (85.3ºN 152ºE and 44 km in diameter) have large amounts of permanent shadow.

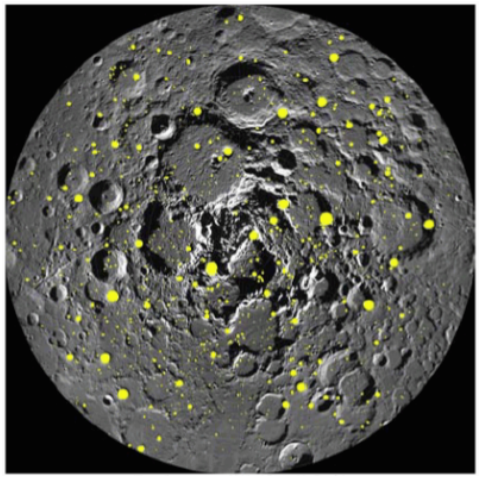

Figure 4.7 Craters mapped on the lunar North Pole, from 78º N to the pole [41]

Nonetheless, not only at the poles exist permanent shadowed areas, but also at latitudes as low as 58º for both lunar hemispheres. In Figure 4.8, there are the locations of the 51 regions where permanent shadow can be found at the north hemisphere.

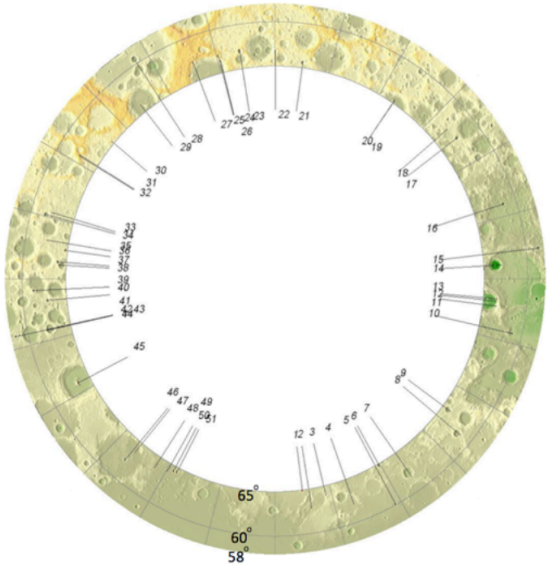

Figure 4.8 Areas of permanent shadow numbered from 58º N to 65º N [42]

In the South Pole, Bussey [41] also mapped 547 craters, with a total surface of 11200 km^2, from where 6500 km^2 are in permanent shadow within 12º of the pole. Some craters like Scott E (81.1ºS 36º W and 28 km in diameter), Idelson L (84.2ºS 116ºE 28 km and in diameter) and Weichert (85.6ºS 177ºW 34 km and in diameter) have large amounts of permanent shadow. But also there others in constant shadow like Haworth (86.9ºS 4ºW and 35 km in diameter), Shoemaker (88.1ºS 44.9ºE and 51 km in diameter), Shackleton (89.63ºS 132.32ºE and 21 km in diameter) and Faustini (87.3ºS 77ºE and 39 km in diameter).

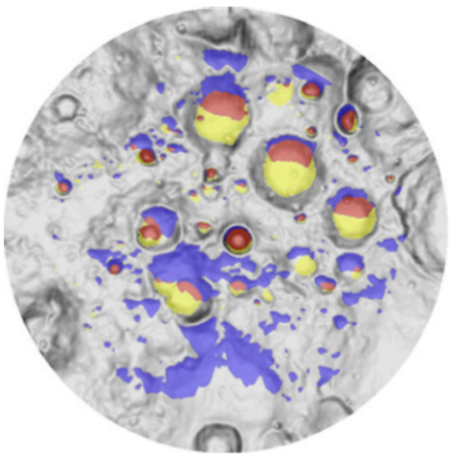

Figure 4.9 A permanent shadow map within 4º of the south pole. Areas in yellow and red are Sun shadowed, areas in red are Sun and Earth shadowed and areas in blue or red are Earth shadowed. [36]

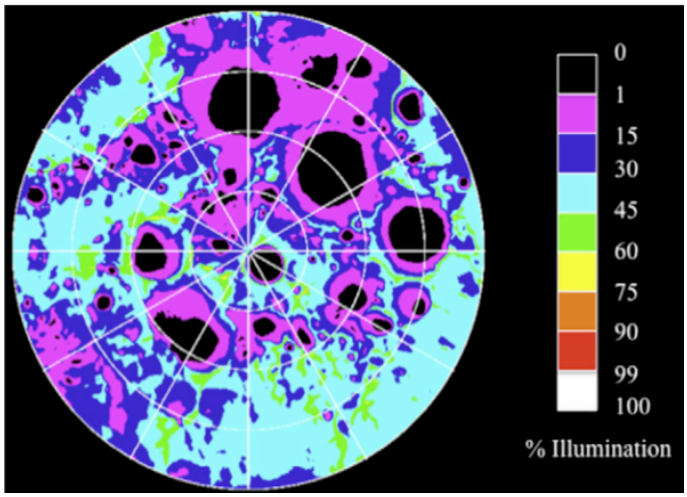

Figure 4.10 A quantitative illumination map within 4º of the south pole during the year 2020 [36]

4.2.2.2. Far side

The farside of the Moon offers isolation from radio transmissions from the Earth, so the IAA (International Academy of Astronautics) and the scientific community [43] have proposed to keep the Moon free man-made RFI and reserve it only for scientific purposes.

They propose to create the Protected Antipode Circle (PAC) [34], which is a circular piece of land of about 1820 km in diameter, centered around the Antipode on the Farside of the Moon. Specifically crater Daedalus (5.9°S 179.4°E and 93 km in diameter) is ideal to set up a future radio telescope to detect radio waves of all kinds that it is impossible to detect on Earth because of the RFI.

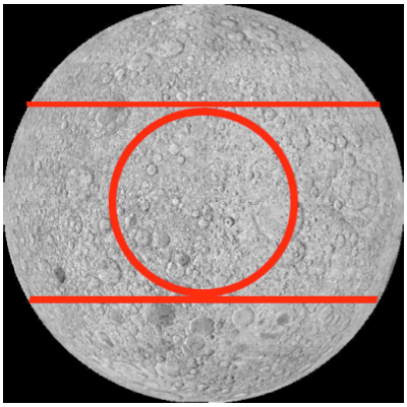

Figure 4.11 Location of the Protected Antipode Circle on the Farside of the Moon [43]

PAC is the only area of the farside that will never be reached by the radiation emitted by future human space bases located at the L4 and L5 Lagrangian points of the Earth-Moon system.

It is also the most shielded area of the Farside, with an expected attenuation of man-made RFI ranging from 15 to 100 dB or higher.

And finally, it does not overlap with other areas of interest to human activity except for a minor common area with the Aitken Basin, which is a huge impact crater of about 2500 km in diameter and 13 km deep on the South Pole.

CONCLUSIONS

An Electrodynamic Screen (EDS) concept has been characterized in order to prevent lunar dust from depositing on the surface of solar panels and optical elements ~~since it is a good candidate because no mechanical action or water are involved~~. A three-phase EDS is chosen, with square vertical configuration for solar panels and circular vertical for optics.

The proper configuration of an EDS depends on the AC signal that feeds the shield and the size distribution of the lunar dust. Therefore analyzing different experiments conducted to date, we have found that the amplitude of the AC signal should be comprised between 6 and 8 kV, its frequency in the range of 5 and 15 Hz and the signal should have a pulsed waveform.

The particles diameter influence on the width of the electrodes and the distance between them. The best configuration is when the inter-electrode spacing is the range of 500 and 750 μm, and the width between 50 and 100 μm. The material of the electrodes could be ITO, AZO or CNT.

Then, the best location for solar panels and telescopes has been assessed. Lunar poles, where there is near-constant illumination, are perfect to settle solar panels. In particular, near the Peary crater in the north with 89% of illumination, and near Shackleton crater in the south with 86%.

Regarding telescopes, choosing just one place is more difficult since it depends on its mission. If a telescope needs cryogenic temperatures, it will be placed on deep craters placed on the poles, where the Sun never rises. If it wants to avoid radio noise, the best place is the far side and if it needs communication with the Earth, the limb is better.

These locations, nevertheless, are not exempt from the lunar dust problem. The height at which the instruments should be placed to mitigate the accumulation of dust is linked to the dynamic dust fountain model.

Solar panels should be at a minimum height of 2 m to avoid the terminator and the horizon glow, always present in the polar regions. As well as almost all dust, with size distribution greater than 1 or 2 μm , levitate up to 2 m maximum in the illuminated areas.

On the other hand, telescopes can be placed in a very wide range of sites along the Moon’s surface, even in constant shadowed craters, where dust levitates from 10 to 100 m. However, the horizon glow is still present, thus, in order to avoid it and to reduce the accumulation of dust; optics should be 1 or 2 m above the surface. Thereby the EDS can be activated less often, saving energy and mitigating the dust diameter that may deposit on the shield.

Finally, the information provided herein is based in literature analysis and experiments performed to date. We suggest that, in order to better characterize the

EDS performance in the lunar environment, ~~a~~ future work could focus on the development of a demonstrator to reduce the width of the electrodes and the spacing between them and also to prove which material offer the better performance of the shield. Moreover, at present there is a NASA lunar exploration mission called *Lunar Atmosphere and Dust Environment Explorer* (LADEE), to better characterize the lunar dust, thus it will shed new light on the size distribution of lunar dust and its residence time on the tenuous exosphere of the Moon.

BIBLIOGRAPHY

[1] L. Taylor, H. Schmitt, W. Carrier, and M. Nakagawa, "Lunar Dust Problem: From Liability to Asset", *1st Space Exploration Conference: Continuing the Voyage of Discovery*, AIAA2005-2150, Vol. 1 (2005).

[2] L. H. Lee, "Adhesion and Cohesion Mechanisms of Lunar Dust on the Moon's Surface", 73-94, in *Fundamentals of Adhesion and Interfaces*, Eds: D. S. Rimai, L. P. DeMejo and K. L. Mittal (1995).

[3] J. R. Cain, "Lunar dust: The Hazard and Astronaut Exposure Risks", *Earth. Moon. Planets*, vol. 107 (1), 107–125 (2010).

[4] J. E. Colwell, S. Batiste, M. Horányi, S. R. Robertson, and S. Sture, "The Lunar Surface: Dust Dynamics and Regolith Mechanics", *Reviews Geophysics*, vol. 45 (2), RG2006 (2007).

[5] J. Park, Y. Liu, K. D. Kihm, and L. A. Taylor, "Characterization of Lunar Dust for Toxicological Studies I: Particle Size Distribution", *J. Aerosp. Eng.*, 266–271 (2008).

[6] Y. Liu, J. Park, D. Schnare, E. Hill, and L. A. Taylor, "Characterization of Lunar Dust for Toxicological Studies II: Texture and Shape Characteristics", *J. Aerosp. Eng.*, 272–279 (2008).

[7] C. M. Katzan, and J. L. Edwards, Report, "Lunar Dust Transport and Potential Interactions With Power System Components", *NASA Contractor Report 4404* (1991).

[8] C. Meyer, "The Lunar Sample Compendium", *Astromaterials Research & Exploration Science* (2010).

[9] M. K. Mazumder, C. I. Calle, K. Pruessner, R. Sharma, P. K. Srirama, M. Ali, C. Immer, S. Trigwell, J. S. Clements, A. S. Biris, J. Mantovani, and A. Chen, "Research needs in electrostatics for Lunar and Mars space missions", *Fourtieth IAS Annu. Meet. Conf. Rec. 2005 Ind. Appl. Conf. 2005,* vol. 1, 327–333 (2005).

[10] T. J. Stubbs, R. R. Vondrak, and W. M. Farrell, "Impact of Lunar Dust on the Exploration Initiative", *36th Lunar and Planetary Science Conference,* Abstract #2277 (2005).

[11] T. J. Stubbs, "Characterizing the Near-Lunar Plasma Environment" *38th Lunar and Planetary Science Conference* (2007).

[12] E. Colwell, S. R. Robertson, M. Horányi, X. Wang, A. Poppe, and P. Wheeler, "Lunar Dust Levitation", *J. Aerosp. Eng.*, vol. 22 (1), 2–9 (2009).

[13] T. J. Stubbs, R. R. Vondrak, and W. M. Farrell, "Impact of Dust on Lunar Exploration", *Workshop on Dust in Planetary Systems (ESA SP-643),* Eds: H. Krueger and A. Graps, 239-243 (2005).

[14] T. J. Stubbs, R. R. Vondrak, and W. M. Farrell, "A dynamic fountain model for lunar dust", *Adv. Sp. Res.*, vol. 37 (1), 59–66 (2006).

[15] C. I. Calle, C. R. Buhler, M. R. Johansen, M. D. Hogue, and S. J. Snyder, "Active dust control and mitigation technology for lunar and Martian exploration", *Acta Astronaut.*, vol. 69 (11–12), pp. 1082–1088 (2011).

[16] S. W. Johnson, G. J. Taylor and J. P. Wetzel, Environmental Effects on Lunar Astronomical Observatories, *"The 2nd Conference on Lunar Bases and Space Activities of the 21st Century"*, Johnson Space Center (NASA), Vol. 1, 329-335 (1992).

[17] S. Biris, D. Saini, P. K. Srirama, M. K. Mazumder, R. A. Sims, C. I. Calle, and C. R. Buhler, "Electrodynamic removal of contaminant particles and its applications", *Conf. Rec. 2004 IEEE Ind. Appl. Conf. 2004. 39th IAS Annu. Meet.*, vol. 2, 1283–1286 (2004).

[18] C. Calle, "Electrodynamic Dust Shield Technology", *NASA Kennedy Space Center.* Retrieved September 19, 2013, from http://empl.ksc.nasa.gov/CurrentResearch/ElectrodynamicScreen/Electrodynamic.htm

[19] E. Johnson, P. K. Srirama, R. Sharma, K. Pruessner, J. Zhang, and M. K. Mazumder, "Effect of particle size distribution on the performance of electrodynamic screens", *40th IAS Annu. Meet. Conf. Rec. 2005 Ind. Appl. Conf. 2005.*, vol. 1, 341–345 (2005).

[20] K. Mazumder, R. A. Sims, J. D. Wilson, "Transparent Self-cleaning Dust Shield", *Patent No. US 6,911,593 B2* (2005).

[21] C. I. Calle, C. R. Buhler, J. L. McFall, and S. J. Snyder, "Particle removal by electrostatic and dielectrophoretic forces for dust control during lunar exploration missions", *J. Electrostat.*, vol. 67 (2–3), 89–92 (2009).

[22] H. Kawamoto, M. Uchiyama, B. L. Cooper, and D. S. McKay, "Mitigation of lunar dust on solar panels and optical elements utilizing electrostatic traveling-wave", *J. Electrostat.*, vol. 69 (4), 370–379 (2011).

[23] M. K. Mazumder, "Self-Cleaning Solar Panels and Concentrators with Transparent Electrodynamic Screens", *Patent No. US 20132/0263393 A1* (2013).

[24] J. P. Bock, J. R. Robison, R. Sharma, J. Zhang, and M. K. Mazumder, "An Efficient Power Management Approach for Self-Cleaning Solar Panels with Integrated Electrodynamic Screens", *Proc. ESA Annual Meet. On Electrostatics Paper O2* (2008).

[25] J. R. Robison, R. Sharma, J. Zhang, and M. K. Mazumder, "Computer Simulation of Electrodynamic Screens for Mars Dust Mitigation", *Proc. ESA Annual Meet. On Electrostatics Paper A3* (2008).

[26] D. Angmo and F. C. Krebs, "Flexible ITO-free polymer solar cells," *J. Appl. Polym. Sci.*, vol. 129 (1), 1–14 (2013).

[27] T. Minami, "Transparent Conducting Oxide Semiconductors for Transparent Electrodes", *Semiconductor Science and Technology* (2005).

[28] "Indium", *Metal Prices*. Retrieved January 7, 2014, from www.metal-pages.com

[29] M. A. Aegerter, "Transparent conducting ATO, ITO and AZO coatings by sol-gel process". Retrieved February 17, 2014, from http://www.solgel.com/labfoc/inm/dipco_e.html

[30] "6 Month Zinc Prices and Price Charts", *InvestmentMine*. Retrieved January 7, 2014, from www.infomine.com

[31] J. Sun and R. Wang, "Carbon Nanotube Transparent Electrode", Chap. 14 in *Syntheses and Applications of Carbon Nanotubes and their Composites,* Ed. S. Suzuki, 313-335 (2013).

[32] R. A. Sims, A. S. Biris, J. D. Wilson, C. U. Yurteri, M. K. Mazumder, C. I. Calle, and C. R. Buhler, "Development of a Transparent Self-Cleaning Dust Shield for Solar Panels," *Proc. ESA-IEEE Joint Meet. On Electrostatics 2003*, 1–8 (2003).

[33] J. Burns and W. W. Mendell, "Future Astronomical on the Moon", *NASA Conference Publication 2489*, Texas (1986).

[34] H. Noda, H. Araki, S. Goossens, Y. Ishihara, K. Matsumoto, S. Tazawa, N. Kawano and S. Sasaki, "Illumination conditions at the lunar polar regions by KAGUYA(SELENE) laser altimeter", *Geophysical Research Letters*, Vol. 35 (24), L24203 (2008).

[35] H. Graem, "Moonbases", *Visions 2200*. Retrieved January 7, 2014, from http://visions2200.com/SpaceLunaMoonbases.html

[36] D. B. J. Bussey, J. a. McGovern, P. D. Spudis, C. D. Neish, H. Noda, Y. Ishihara, and S.-A. Sørensen, "Illumination conditions of the south pole of the Moon derived using Kaguya topography", *Icarus*, vol. 208 (2), 558–564 (2010).

[37] J. M. Carrasco, J. Bernabeu and E. Colell", "The Moon as an Astronomical Platform", *Proc. 4th Int. Conf. Exploration and Utilisation of the Moon,* ESTEC, Noordwijk (The Netherlands), ESA SP-462, 79-86 (2000).

[38] "Astrophysics from the Moon's Advantages" *International Lunar Observatory.* Retrieved November 21, 2013, from http://www.spaceagepub.com/ilo/ilo.home.html

[39] Astronomy and Astrophysics Survey Comittee, Board on Physics and Astronomy, and National Research Council, "Astronomy from the Moon", Chap. 6 in *The Decade of Discovery in Astronomy and Astrophysics,* 100-109 (1991).

[40] R. L. Staehle. J. D. Burke, G. C. Snyder, R. Dowling and P. D. Spudis, "Lunar Base Siting", Chap. 16 in *Resources of Near-Earth Space,* J. Lewis, M. S. Matthews and M. L. Guerrieri, 427-446, Arizona (1993).

[41] D. B. J. Bussey, "Permanent shadow in simple craters near the lunar poles," *Geophys. Res. Lett.*, Vol. 30 (6) (2003).

[42] D. B. J. Bussey, J. T. S. Cabill, J. A. McGovern and P. D. Spudis, "A Global Catalogue of Lunar Permanently Shadowed Regions", *EPSC*, Vol. 7 (2012).

[43] C. Maccone, "PAC at the Center of the Farside of the Moon for the Benefit of all the Humankind", Chap.1 in *Protected Antipole Circle on the Lunar Farside*, IAA, 2–11 (2012).